

ASSESSMENT OF BURNOUT PERFORMANCE OF A CONCRETE BEAM USING A NOVEL ELECTRIC RADIANT PANEL

Balša Jovanović¹, Robby Caspeele², Edwin Reynders³, Geert Lombaert⁴, Florian Put⁵, Andrea Lucherini⁶,
Ruben Van Coile⁷

ABSTRACT

This study investigates the behaviour of a concrete beam exposed to a natural fire by means of experiments using a novel electric radiant panel and simulations using Finite Element Modeling (FEM). In the experimental program, a reinforced concrete beam was tested for deflection, deformation, and temperature changes considering exposure to a heat flux as given by the Eurocode Parametric Fire Curve. The radiant panel enabled precise heat flux control and accurate application of the intended exposure, also in the cooling phase. FEM simulations corroborated experimental data, demonstrating accurate prediction of thermal effects and beam behaviour during fire exposure. It is concluded that the novel test method offers a practical approach for studying the fire response of concrete elements. The results highlight the electric radiant panel's effectiveness in fire simulation and the value of FEM in assessing the structural performance in fire scenarios.

Keywords: Fire testing, Radiant panel, Concrete beam, Numerical modelling

1 INTRODUCTION

Because the traditional fire resistance paradigm does not consider structural performance in the decay and cooling phases, it does not provide direct insight into the performance of structures in real fires [1] [2]. This lack of understanding can be addressed through experimental testing, where structures are examined under full-scale fire conditions, including heating and cooling phases. Although large-scale testing offers deep insights into the damage caused by fire, such tests are generally costly and logistically challenging. The repeatability of these tests is hard to ensure due to the complexity of controlling the fire exposure precisely. Additionally, adhering to specific cooling phases can be problematic, which limits the tests' applicability [3].

Consequently, there is a growing interest in developing techniques to directly manage the thermal conditions applied to test samples. An example is the H-TRIS system [4], which employs a gas-powered

¹ PhD student, Department of Structural Engineering and Building Materials, Ghent University, Belgium
Department of Civil Engineering, Structural Mechanics Section, KU Leuven, Belgium,
e-mail: Balsa.Jovanovic@ugent.be, ORCID: <https://orcid.org/0000-0001-5200-5848>

² Professor, Department of Structural Engineering and Building Materials, Ghent University, Belgium,
e-mail: Robby.Caspeele@ugent.be, ORCID: <https://orcid.org/0000-0003-4074-7478>

³ Professor, Department of Civil Engineering, Structural Mechanics Section, KU Leuven, Belgium,
e-mail: Edwin.Reynders@kuleuven.be, ORCID: <https://orcid.org/0000-0002-1042-0282>

⁴ Professor, Department of Civil Engineering, Structural Mechanics Section, KU Leuven, Belgium,
e-mail: Geert.Lombaert@kuleuven.be, ORCID: <https://orcid.org/0000-0002-9273-3038>

⁵ PhD student, Department of Structural Engineering and Building Materials, Ghent University, Belgium
e-mail: Florian.Put@UGent.be, ORCID: <https://orcid.org/0000-0002-4522-9015>

⁶ PhD, Senior Researcher, Slovenian National Building and Civil Engineering Institute (ZAG), Slovenia
e-mail: Andrea.Lucherini@zag.si, ORCID: <https://orcid.org/0000-0001-8738-1018>

⁷ Professor, Department of Structural Engineering and Building Materials, Ghent University, Belgium,
e-mail: Ruben.VanCoile@ugent.be, ORCID: <https://orcid.org/0000-0002-9715-6786>

radiant panel that can precisely control the applied heat flux to the sample by adjusting the distance between the panel and the sample. Fire testing using electrical pads have been recently presented in [5], however, the electrical pads highlighted shortcomings related to the maximum temperature that could be accurately controlled and therefore the range of the heat flux that could be applied on the test sample. This study utilizes a similar approach but with a very high intensity and fast reponse electric radiant panel. The panel is designated as the HIFREP (High-Intensity Fast-Response Electric Panel) and enables to cover the typical range of heat flux for fire testing. Its composition and capabilities are presented in [6]. More specifically, the feasibility of performing large-scale structural (i.e., loaded) tests using the HIFREP is demonstrated in the following, in a case study of a concrete beam. The objective is to monitor the structural behaviour of the beam, such as deflections, deformations, and temperature variations, during the heating and cooling phase. Complementing this experimental approach, Finite Element Modeling (FEM) is employed to offer a detailed analysis of the structural responses, enhancing the insights obtained experimentally.

2 EXPERIMENTAL PROGRAM

2.1 Beam description

The beam measures 3.8 meters in length, with a cross-sectional height of 290 mm and a width of 200 mm. Reinforcement includes five steel rebars, each 16 mm in diameter. Of these, three rebars are placed in the beam's tension zone, with the remaining two situated in the compression zone. The concrete cover is 20 mm. This limited cover is chosen intentionally to enhance the structural effect of the thermal loading while limiting the total exposure time to a manageable duration. For shear reinforcement, 8 mm stirrups are utilized, arranged at intervals of 200 mm over the beam's length. The concrete used has a C30/37 concrete class and the reinforcement is B500B grade steel. The constituents of the concrete mix used for the beam are listed in Table 1. The design moment capacity is 61.6 kNm, determined in accordance with [7].

Table 1 Concrete mix constituents

Materials	Weight [kg/m ³]	Ratio to cement [-]
Cement	340	1.00
Aggregate	1780	5.23
Water	187	0.55

The mean compressive strength result for the sample concrete cubes is $f_{c,cube} = 45.7 \text{ MPa}$ with a standard deviation of 2.0 MPa. The measured mean yield strength of the reinforcement is $f_y = 565 \text{ MPa}$ and the mean value of the modulus of elasticity is $E_s = 213 \text{ GPa}$.

2.2 Panel description

To simulate the conditions of fire exposure for this experiment, a novel electric radiant panel with high-intensity output is utilized, i.e., the HIFREP. The panel is made up of 21 emitters, each 500 mm long, which emit high-intensity, short-wavelength infrared radiation. Together, these emitters span an area of about 900 mm by 500 mm and are shielded by a detachable transparent quartz glass panel. At full power, the panel is capable of producing a nearly uniform radiative heat flux of 100 kW/m² over a targeted area of 200 mm by 700 mm, located 100 mm away from the glass protector. The variation in radiative heat flux across this area, relative to that at the central position, is depicted in Figure 1.

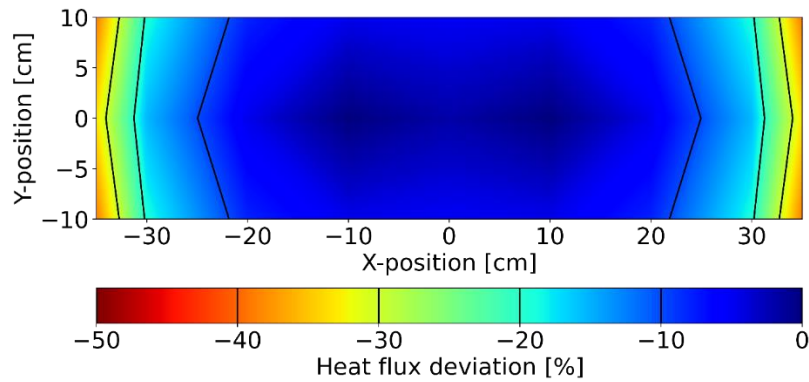


Figure 1 Received heat flux deviation compared to the central position over the exposed beam area, for the panel positioned at a 100 mm distance.

Precise control of the panel's radiation intensity is managed by adjusting the voltage as an input signal. This precise control enables the fine adjustment of the radiative heat flux experienced by the specimen, mirroring the total heat flux a specimen would face in a fire scenario, encompassing the heating, decay and cooling phases [8]. This control is implemented via a custom Python program on a computer, facilitating the real-time modification and tracking of the radiant heat flux.

2.3 Setup description

A reversed four-point bending setup was employed to apply mechanical loading, inverting the usual configuration for enhanced safety during the heating phase (Figure 2). The beam supports were symmetrically placed from the beam's centre, spaced 2100 mm apart. Loads were applied 100 mm from the beam's edges, which translates to 750 mm from where the supports were positioned. This inverted arrangement offered multiple benefits. It positioned the beam's tensioned side upwards, optimizing the exposure to the radiant panel's heat flux for safety and efficacy. Moreover, this setup maintained the displacements caused by the heat in proximity to the panel to a low level, reducing the need for adjustments due to beam bending.

The central section of the beam, spanning 700 mm, was directly subjected to the panel's radiative heat flux. This specific section is characterized by a uniform bending moment, aside from the effects of the beam's own weight. To isolate the heating effect within this zone, insulation boards were placed over the top sections of the beams not intended for heating. Additionally, the beam's lateral surfaces were shielded with insulation boards to minimize thermal losses in these areas, as illustrated in Figure 3. This setup was designed to create conditions approximating one-dimensional heat transfer over the beam's height, as much as possible eliminating lateral heat losses. This then allows for a simple adiabatic surface condition at the beam's sides in a thermal analysis of the beam.

2.4 Instrumentation

Vertical displacements were recorded using Linear Variable Differential Transformers (LVDTs) placed beneath the load application points and at the beam's midpoint, specifically on the side shielded from the radiant panel. Additionally, Digital Image Correlation (DIC) was employed for capturing displacement data in the beam's central region. The use of insulation boards and the radiant panel's intense illumination meant that displacement measurements through DIC were confined to the beam's lower half, i.e. the side under compression, as depicted in Figure 4. For processing these images, VIC-3D software by Correlated Solutions was utilized [9].

Temperature variations within the beam were measured by casting 18 type-K thermocouples. These sensors were distributed across three key areas along the beam's length: the centre and two neighbouring sections, each 300 mm from the midpoint, as indicated in Figure 7. At these points, six thermocouples were installed at varying depths from the surface facing the heat: at 12 mm (in the middle of the shear reinforcement), 20 mm (connection of the main and shear reinforcement in the tension zone), 50 mm, 100 mm, 150 mm and 278 mm. These thermocouples were fixed using 2 mm thick steel wires attached to the reinforcement cage, ensuring their stability throughout the casting process.

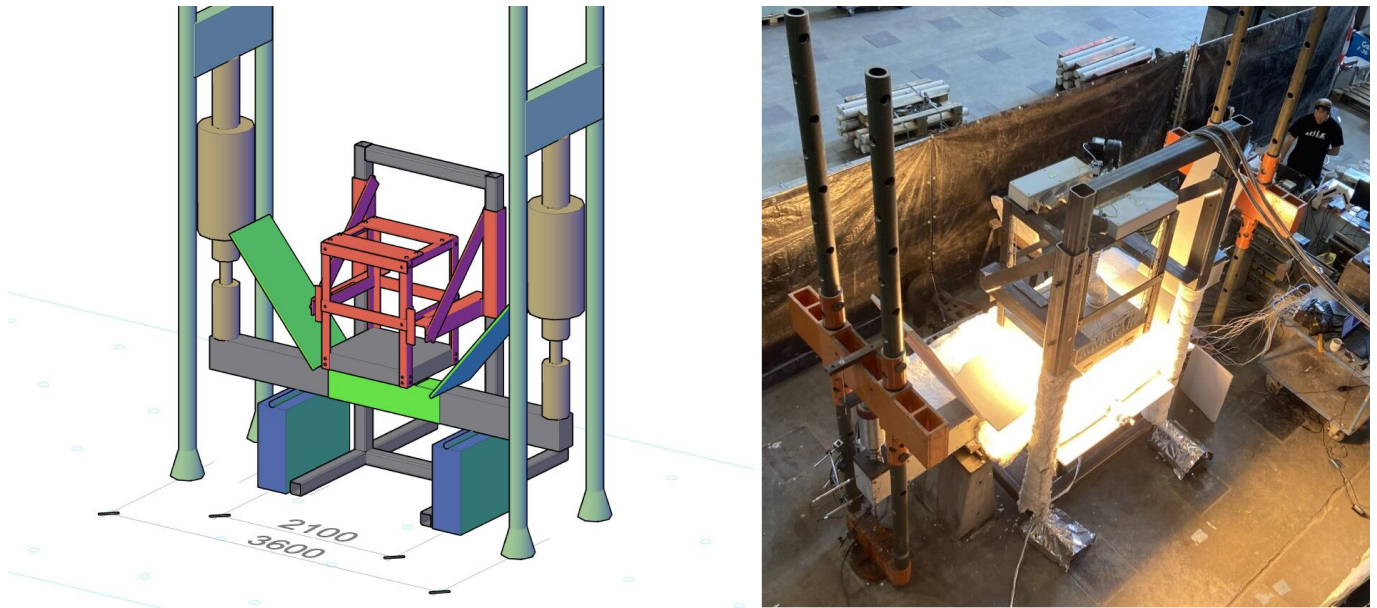


Figure 2. Test setup schematic overview (left); picture of the actual test set-up (right).

2.5 Fire exposure

The experiment replicated natural fire conditions by adhering to the Eurocode Parametric Fire Curve (EPFC) [10]. Specifically, an EPFC variant with a Γ value of 0.45 and a heating phase set to last 1 hour was adopted. This specific EPFC variant predicts a peak “gas” exposure temperature of 826 °C and a total fire exposure duration of 233 minutes. The radiant panel's heat flux was calculated to mirror the EPFC's total heat impact on the beam's surface. Achieving a maximum radiative heat flux of 85.75 kW/m², the application of heat was discontinued at the 155-minute mark, coinciding with the moment when the needed panel intensity is lower than 10% of its maximum power. Illustrations of the targeted temperature-time trajectory and the heat flux applied are provided in Figure 5.

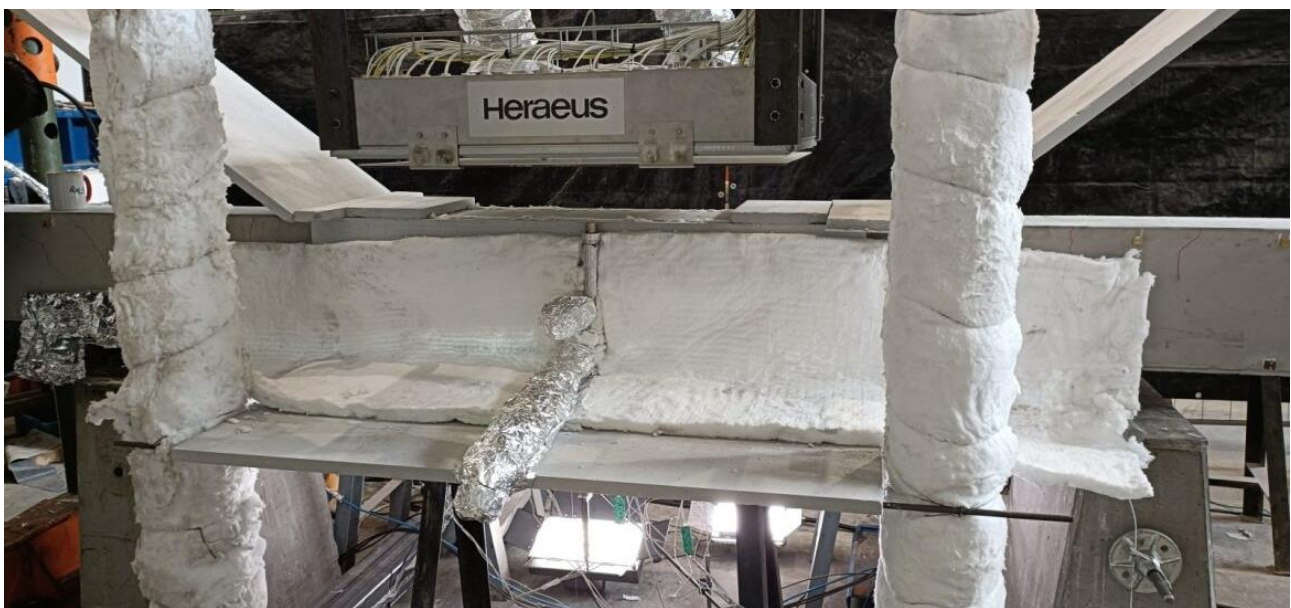


Figure 3. Insulation protection on the beams.



Figure 4. The compressed side of the beams monitored using the Digital Image Correlation (DIC).

Throughout the testing process, the beam's surface heat flux was measured using a water-cooled Schmidt-Boelter heat flux meter. This device was placed next to the beam, aligned with the surface at the central part of the heat exposure area. To accommodate the beam's potential deformation, the heat flux meter was attached in a manner that maintained its alignment with the beam's surface. The outcome of this measurement is detailed in Figure 6. Notably, the recorded heat flux values exceeded the predetermined target. This discrepancy is largely ascribed to convective heat transfer from the surrounding warm air impacting the heat flux meter. By estimating the convective heat transfer coefficient at approximately $20 \text{ W}/(\text{m}^2\text{K})$ and assuming that the air temperature near the meter approximately matches the targeted concrete surface temperature, an adjustment was made to the measured heat flux values. This adjusted comparison suggests that the beam's surfaces indeed were subject to the planned radiative heat flux levels.

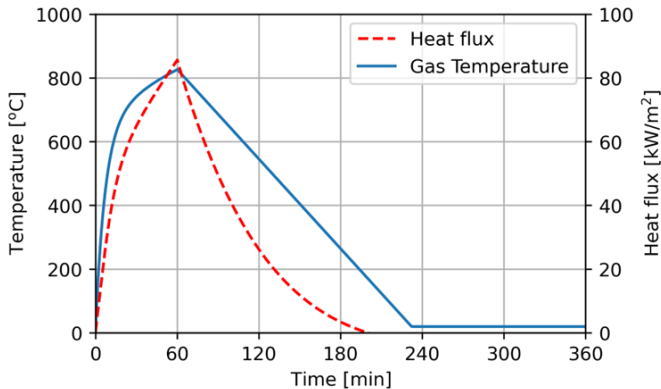


Figure 5 Eurocode Parametric Fire Curve temperature-time curve and equivalent radiant heat flux from the panel.

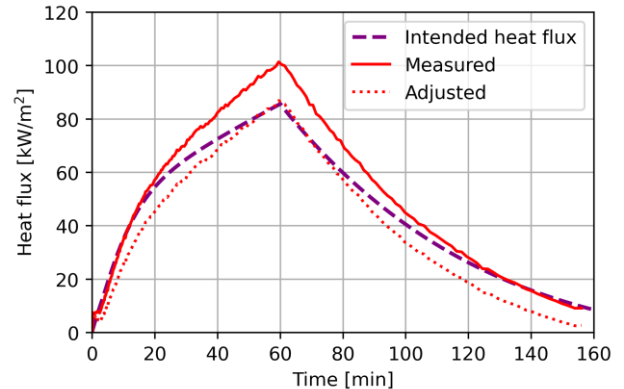


Figure 6 Measured and intended radiative heat flux during the tests. After 155 min, the panel was shut down and the beam was allowed to cool naturally.

3 EXPERIMENTAL RESULTS

As outlined in Section 2.4, the internal temperatures of the beam were monitored at three longitudinal points along their length, employing six thermocouples embedded within the beam at each location depicted in Figure 7. The temperatures recorded at depths of 20 mm, 50 mm, and 150 mm from the beam's surface that faced the heat are showcased in Figure 8. This figure reveals that the heating effect was evenly distributed, as indicated by the nearly identical temperatures on both the left and right sides of the zone subjected to heat. Nevertheless, temperatures at the central part were observed to be higher, attributed to the radiative heat flux's imperfect uniformity over the exposed area (as seen in Figure 1) and the greater impact of heat conduction towards the beam's cooler sections. This pattern of temperature distribution was consistently observed at every depth measured by the thermocouples.

Figure 9 provides a visual representation of the temperature variations within the beam's core over time, achieved through linear interpolation of temperature data from various depths. This approach aids in illustrating the temperature gradient throughout the beam. Notably, the data also indicate that temperatures

within the beam continue to rise beyond the 60 minutes of the heating phase, penetrating deeper into the beam as anticipated. It highlights that the temperature readings at all three monitored positions remain relatively consistent with one another. The most notable variances occur near the beam's surface, particularly at a depth of 12 mm, where the thermal gradient is most pronounced. Minor shifts in the placement of thermocouples at this shallow depth can markedly influence the recorded temperatures. Despite this sensitivity, the disparity in temperature readings remains within a 10% margin, underscoring the precision of the measurements. For deeper positions within the beam, the temperature differences become virtually inconsequential, indicating uniform thermal behaviour throughout the structure's cross-section under fire exposure conditions.

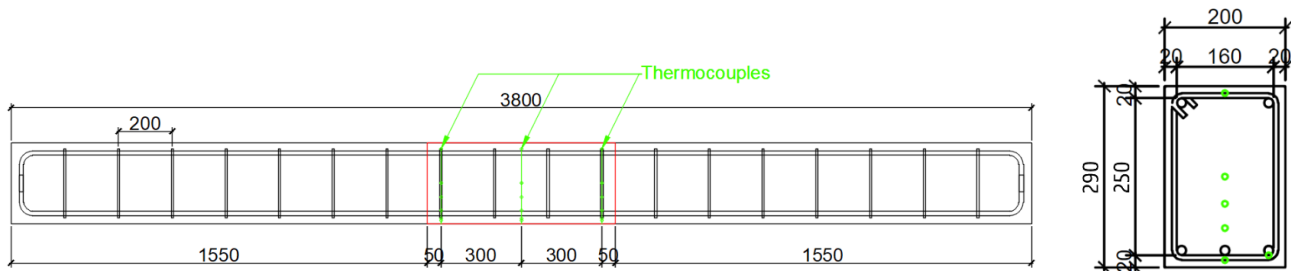


Figure 7. Position of the thermocouples cast inside the beams in the longitudinal direction and in the cross-section (red box represents the heated area) (dimensions in mm)

The panel was deactivated after 155 minutes, and the radiative heat flux dropped to below 10% of its peak value. This transition is visible in Figure 13 as the shutdown marks a change in thermal boundary conditions: with the end of radiative heat, the surface begins to cool through convection. This quasi-immediate cooling effect is particularly noticeable at shallower depths of 12 and 20 mm, whereas at greater depths, its impact is minimal.

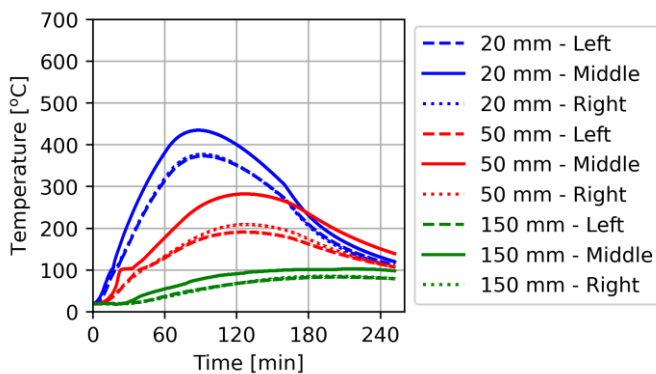


Figure 8 Measured temperatures at different depths and positions during the test.

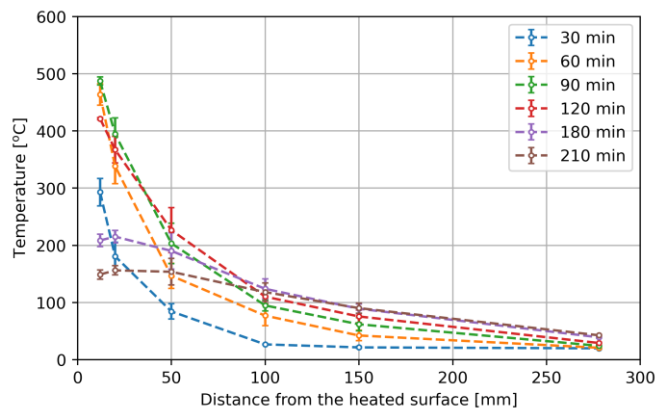


Figure 9. Thermal gradient inside of the beam at different points in time (error bar represents the standard deviation between three positions).

Figure 10 illustrates the midspan deflection recorded during the testing. These deflections are depicted relative to their initial state at the onset of the heating phase, with a baseline (0 mm) representing the deflection under the serviceability load before heating commenced. In the initial 60 minutes, correlating with the period of increasing heat flux, the deflections display an almost linear rise. This upward trend in deflections decelerates but persists until about 95 minutes, at which point the beam achieves its peak deflection. Following this peak, the deflections maintain a near-constant level for around 15 minutes before gradually declining. This reduction pattern in deflections mirrors the temperature behaviours observed; notably, the deflection decrease rate alters once the heating panel is deactivated at 155 minutes.

Figure 11 displays the average displacements occurring under the points where loads were applied during the tests. The pattern of deformation observed under the load application points mirrors that of the midspan deflections. Employing Digital Image Correlation (DIC) allowed for the detailed assessment of curvature across the zone subjected to a uniform moment. The resulting curvature changes within the heated zone are documented in Figure 12.

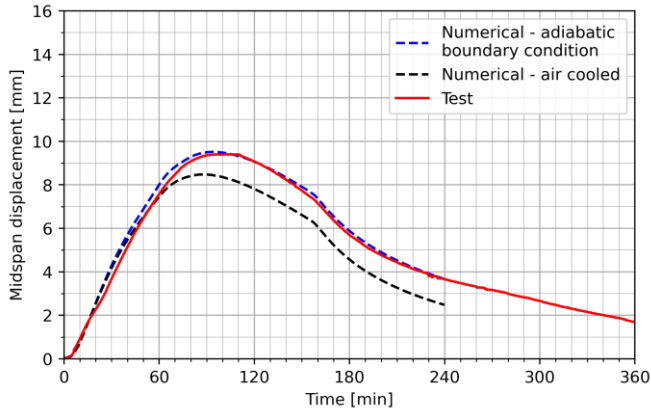


Figure 10. Midspan displacement during the tests compared to the results of numerical simulations

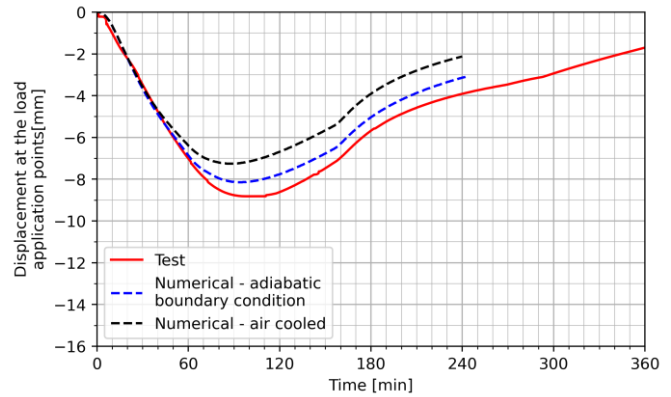


Figure 11 The average displacement at the load application points during the tests compared to the results of numerical simulations.

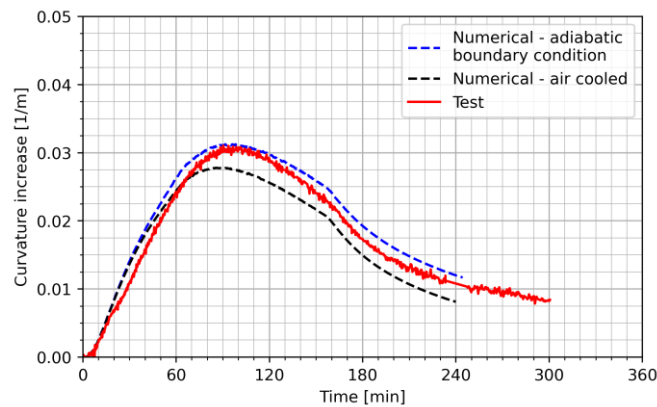


Figure 12. Midspan curvature change observed during the test and numerical simulations.

4 NUMERICAL MODELING

A finite element model for the beam was created using the SAFIR [11] software. This analysis consists of two distinct phases. Initially, a heat transfer analysis was undertaken to produce the temperature-time history of the beam. Subsequently, this temperature-time data serves as an input for the structural analysis, enabling an evaluation of the beam's structural behaviour during the natural fire exposure.

4.1 Heat transfer

The heat transfer analysis employed a two-dimensional model to simulate the temperature changes within the beam's cross-section. The cross-section was segmented into 1320 rectangular elements, their sizes ranging from 4 to 8 mm. To represent the concrete and its steel reinforcement within the model, the materials SILCON_EN for concrete and STEELEC2EN for steel were utilized with their default parameters as stated in EN 1992-1-2 [12]. The model's thermal boundary conditions at the tensioned edge are modelled as both radiative and convective heat transfer from a singular temperature-time profile. Specifically, from

an EPFC characterized by a Γ value of 0.45 and a heating duration of 1 hour, as detailed in Section 2.5 and illustrated in Figure 5.

Upon the panel's deactivation at the 155-minute mark, adjustments were made to the EPFC's cooling trajectory: the EPFC was followed until 155 minutes after which the temperature-time curve was abruptly transitioned to a stable 20 °C. This approach to modelling radiative heat transfer assumed a concrete surface absorptivity/emissivity of 0.7, with convection being modelled with a coefficient of 35 W/(m²K) in accordance with Eurocode guidelines [10, 12]. For the beam's compressed side, where both convective and radiative heat losses were projected against a steady 20 °C ambient temperature, the parameters were set to an emissivity of 0.7 and a reduced convection coefficient of 4 W/(m²K), consistent with Eurocode's recommendations [10, 12]. The described modelling approach thus starts from the exposure intended to be applied with the panel, and not from the measured exposure. It thus constitutes an a priori modelling.

As previously noted, the beam sides were safeguarded against direct radiation through the application of insulation boards. Nonetheless, an air gap of about 15 mm was present between the board and the beam to facilitate instrumentation. This air gap was manually sealed with insulation material at the top. Thus, the air gap was intended to effectively act as an insulator, rendering the boundary condition of the beam's sides akin to perfect insulation. Consequently, this scenario was modelled as an adiabatic boundary condition, assuming no heat transfer through these surfaces.

In Figure 13 the outcomes of the heat transfer analysis are illustrated and compared with the in-situ thermocouple readings from the testing phase. This comparison reveals a strong agreement between the simulated heat transfer behaviours and the empirical temperature measurements across various depths within the beam, underscoring the model's accuracy in replicating the thermal dynamics experienced by the beam under test conditions. The alternative “air-cooled” modelling approach presented in the figure is outlined below in Section 5.

4.2 Structural analysis

In the structural phase of the analysis, the beam was conceptualized as a two-dimensional fibre model spanning 3600 mm, i.e., the distance between points where loads were applied. This model was segmented into 72 elements, each measuring 50 mm in length. Specifically, the central 14 elements were assigned the temperature-time profiles derived from the heat transfer analysis, while the remaining segments of the model were maintained at a constant temperature of 20 °C for the duration of the simulation. The simulation's mechanical boundary conditions mirrored those utilized in the experimental setup, incorporating both roller and pin supports to replicate the test conditions accurately. Loading was simulated by applying two vertical forces, each fixed at 55 kN, positioned at the beam's extremities.

The analysis utilized the SILCON_ETC concrete model, which incorporates the explicit transient creep model introduced in [13]. This model's parameters were aligned with empirically determined material properties, setting the concrete's compressive strength to $f_c = 45.7$ MPa and its tensile strength $f_t = 2.9$ MPa. The reinforcement was represented through the STEELEC2EN model, as outlined in EN 1992-1-2:2004, with a specified yield strength $f_y = 565$ MPa and a modulus of elasticity $E_s = 213$ GPa, reflecting the actual material characteristics measured.

Figure 10 compares the simulated midspan deformations against those observed during experimental testing, showcasing the model's precision in reflecting the beam's experimental behaviour.

5 DISCUSSION

The heat transfer within the model was initially assumed to occur under conditions of perfect insulation. However, the presence of an air gap during experimental testing complicates the accurate modelling of the actual heat loss, due to the complex interaction and cavity effects between the concrete, air and insulation. To investigate this discrepancy, an alternative model was adopted with different boundary conditions at the beam's vertical edges. In this revised model, these edges were considered to be exposed to ambient air, mirroring the cooling conditions applied to the compressed edge of the beam, as depicted in Figure 14. The

comparison of experimental results with the simulation indicates a closer alignment when the side edges are assumed to be adiabatically insulated, particularly within the initial 120 minutes of testing. A noticeable transition towards the conditions simulating exposure to ambient air becomes evident thereafter. This observation could be attributed to the temperature dynamics within the air gap: during the heating phase, the air within this gap warmed up together with the beam, but likely remained colder than the air at the top of the gap. Thus there was no buoyancy-driven air replacement, mitigating any cooling effect on the beam's side. As the beam's temperature began to decrease, the air within the gap became more hot than the air at the top of the gap. Thus, a buoyancy-driven flow likely developed, enhancing the cooling effect on the beam's sides. The impact of these differing boundary conditions on the side edges appears to be minimal at greater depths within the beam.

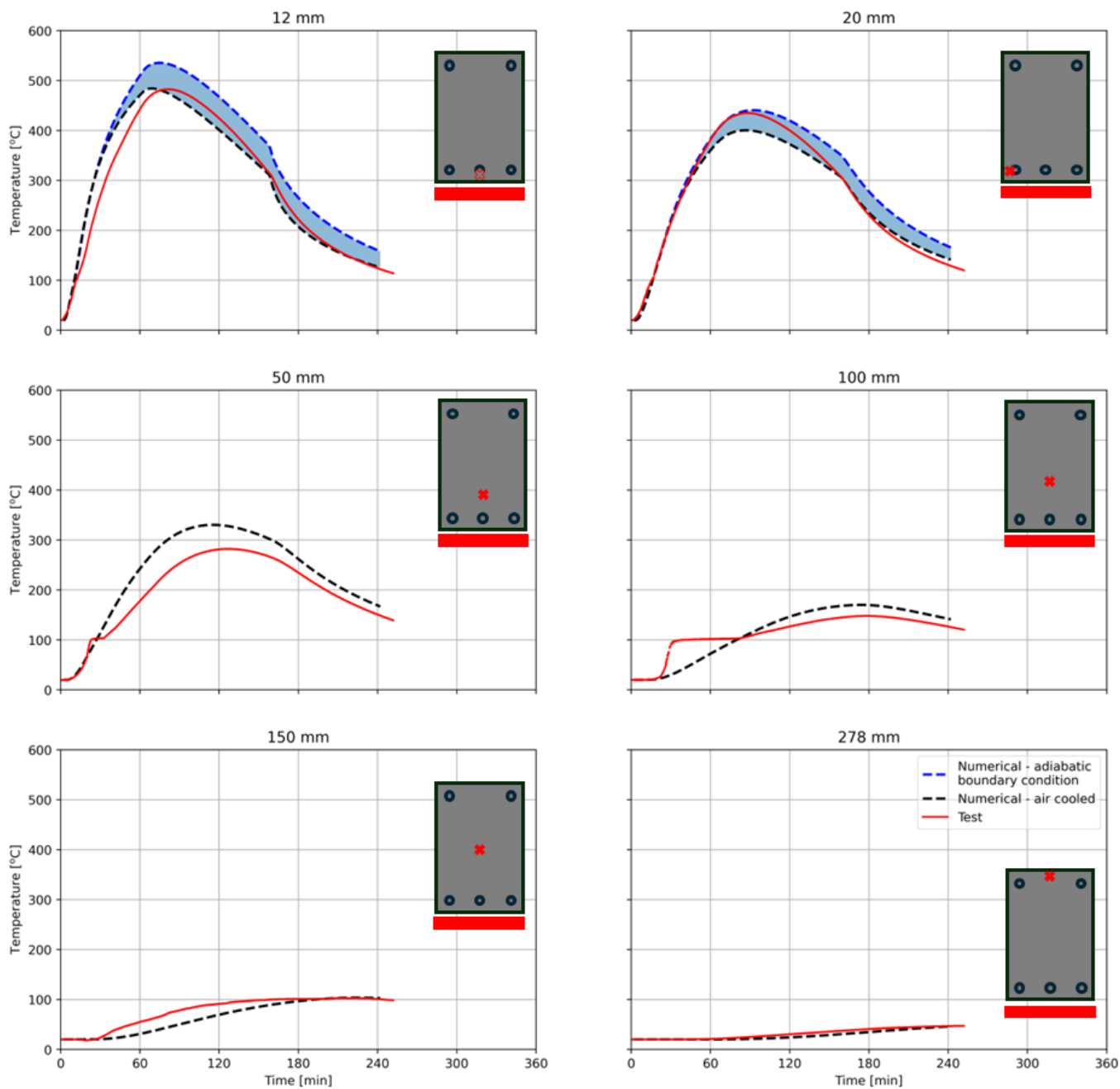


Figure 13. Temperatures at the midspan section measured during the test at different depths compared to the numerical results. A distinction is made between (i) adiabatic and (ii) air-cooled numerical results related to the modelling of the boundary condition for the side of the beam.

When looking at Figure 10, it can be concluded that the correspondence between the numerical simulations and the empirical results of midspan deformations is significantly better when the boundary conditions along the beam's side edges are assumed to be adiabatic. This pattern of similarity extends to the behaviours depicted in Figure 11, which charts the deflection variations at the load application points—essentially, the beam's extremities—throughout the heating and cooling stages. Further, an examination of the mid-span curvature in Figure 12 reveals a very close agreement between the experimental outcomes and the simulation predictions.

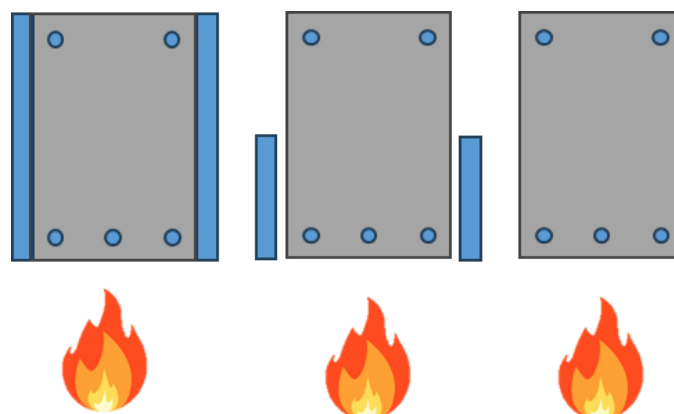


Figure 14. Different cases for modelling boundary conditions on the side edges of the concrete beam: full insulation (left), real scenario during the test (middle; this case is not directly modelled) and ambient air contact (right).

6 CONCLUSIONS

A novel electric radiant panel was employed to replicate the effects of natural fire on a concrete beam. Despite constraints regarding the size of the heated area and the peak heat flux attainable, the panel's performance excelled in terms of control accuracy and the consistency of test conditions.

During the heating phase, the structural behaviour of the beam transitioned through several stages. Initially, deflections increased in a linear fashion, then progressed at a diminished rate until reaching a peak. Following this peak, the beam exhibited a period of stability, maintaining its maximum deflection before the deflections gradually decreased as the beam cooled. This pattern of response is in line with the anticipated behaviour of concrete structures subjected to fire, evidencing a predictable reaction to increasing temperatures.

The Finite Element Method (FEM) analysis that takes into account both the heat transfer and elevated temperature material behaviour, using the SAFIR software, has shown to be a very accurate means of simulating the behaviour of the simply supported concrete beam under natural fire conditions. The model's predictions of how the beam would respond structurally to thermal stress were closely aligned with empirical observations. The difference between the simulated results and the test data was minimal.

The strong correlation between observed temperature measurements and the results from numerical simulations highlights the effectiveness of the experimental setup in accurately replicating conditions as in the Eurocode Parametric Fire Curve's temperature-time profile.

This study contributes to the field of fire engineering by showcasing a novel and environmentally friendly methodology for replicating fire-induced damage in concrete elements. Employing the novel electric radiative panel to mimic real fire conditions accurately presents a viable path for examining how concrete structures behave during exposure to a natural fire with cooling regime.

ACKNOWLEDGEMENTS

The authors wish to thank the Research Foundation of Flanders (FWO) for the financial support on the research project (Grant number 3G010220) “Vibration-based post-fire assessment of concrete structures using Bayesian updating techniques”. Andrea Lucherini is funded by the FRISSBE project within the European Union’s Horizon 2020 research and innovation program (GA 952395) and Florian Put is funded by Research Foundation of Flanders (FWO) within the scope of the research project (Grant number 1137123N) “Characterization of the thermal exposure and material properties of concrete during the fire decay phase for performance-based structural fire engineering”.

REFERENCES

1. Gernay, T.: Fire resistance and burnout resistance of reinforced concrete columns. *Fire Safety Journal*. 104, 67–78 (2019). <https://doi.org/10.1016/j.firesaf.2019.01.007>
2. fib, Fédération International du Béton: fib Bulletin 108. Performance-based fire design of concrete structures. (2023)
3. Gernay, T., Franssen, J.-M., Robert, F., McNamee, R., Felicetti, R., Bamonte, P., Brunkhorst, S., Mohaine, S., Zehfuß, J.: Experimental investigation of structural failure during the cooling phase of a fire: Concrete columns. *Fire Safety Journal*. 134, 103691 (2022). <https://doi.org/10.1016/j.firesaf.2022.103691>
4. Maluk, C., Bisby, L., Krajcovic, M., Torero, J.L.: A Heat-Transfer Rate Inducing System (H-TRIS) Test Method. *Fire Safety Journal*. 105, 307–319 (2019). <https://doi.org/10.1016/j.firesaf.2016.05.001>
5. Seweryn, A., Lucherini, A., Franssen, J.-M.: An Experimental Apparatus for Bench-Scale Fire Testing Using Electrical Heating Pads. *Fire Technol.* (2023). <https://doi.org/10.1007/s10694-023-01514-4>
6. Put, F., Jovanović, B., Evelien, S., Lucherini, A., Merci, B., Van Coile, R.: High-Intensity Fast-Response Electric radiant Panel (HIFREP) for increased accuracy on thermal boundary conditions during fire testing. 4th European Symposium on Fire Safety Science – ESFSS 2024. (in press)
7. CEN: EN 1992-1-1:2004: Eurocode 2: Design of concrete structures - Part 1-1: General. rules and rules for buildings, (2004)
8. Lucherini, A., Torero, J.L.: Defining the fire decay and the cooling phase of post-flashover compartment fires. *Fire Safety Journal*. 141, 103965 (2023). <https://doi.org/10.1016/j.firesaf.2023.103965>
9. Correlated Solutions: Vic-3D, www.correlatedsolutions.com/supportcontent/VIC-3D-8-Manual.pdf, (2010)
10. CEN: EN 1991-1-2:2002 Actions on structures - Part 1-2: General actions - Actions on structures exposed to fire, (2002)
11. Franssen, J.-M., Gernay, T.: Modeling structures in fire with SAFIR®: theoretical background and capabilities. *Journal of Structural Fire Engineering*. 8, 300–323 (2017). <https://doi.org/10.1108/JSFE-07-2016-0010>
12. CEN: EN 1992-1-2:2004: Eurocode 2: Design of concrete structures - Part 1-2: General rules. Structural fire design, (2004)
13. Gernay, T., Franssen, J.M.: A formulation of the Eurocode 2 concrete model at elevated temperature that includes an explicit term for transient creep. *Fire Safety Journal*. 51, 1–9 (2012). <https://doi.org/10.1016/j.firesaf.2012.02.001>